Dynamic characteristics of sulfur, iron and phosphorus in coastal polluted sediments, north China

Qiyao Sun[1], Yanqing Sheng [1*], Jian Yang[1], Marcello Di Bonito[2] and Robert J.G. Mortimer[2]

[1] Research Center for Coastal Environment Engineering Technology of Shandong Province, Yantai Institute of Coastal Zone Research, Chinese Academy of Sciences, Yantai,China

[2] School of Animal, Rural and Environmental Sciences, Nottingham Trent University, Brackenhurst Campus, Southwell, Nottinghamshire, NG250QF, UK

[*] Author to whom correspondence should be addressed; E-Mail: yqsheng@yic.ac.cn (Y.S.); Tel.: +86-535-210-9265; Fax: +86-535-210-9000.

Abstract

The cycling of sulfur (S), iron (Fe) and phosphorus (P) in sediments and pore water can impact the water quality of overlying water. In a heavily polluted river estuary (Yantai, China), vertical profiles of fluxes of dissolved sulfide, Fe^{2+} and dissolved reactive phosphorus (DRP) in sediment pore water were investigated by the Diffusive Gradients in Thin films technique (DGT). Vertical fluxes of S, Fe, P in intertidal sediment showed the availability of DRP increased while the sulfide decreased with depth in surface sediment, indicating that sulfide accumulation could enhance P release in anoxic sediment. In sites with contrasting salinity, the relative dominance of iron and sulfate reduction was different, with iron reduction dominant over sulfate reduction in the upper sediment at an intertidal site but the reverse true in a freshwater site, with the other process dominanting at depth in each case. Phosphate release was

largely controlled by iron reduction.

Capsule:

The relative rates of microbial iron and sulfate reduction controlled the flux of Fe^{2+}, sulfide and phosphate to the pore waters in coastal sediments.

Key words: Sulfur; Iron; Phosphorus; Sediment; DGT

1. Introduction

Sediments play an important role in the evolution of the aquatic environment, as many contaminants from municipal, industrial and non-point sources are associated with solid particles that accumulate as sediments, creating a potential threat to benthic organisms (Dittrich et al., 2013; Sheng et al., 2013). Sediments can also be re-suspended at high flow rates or within estuarine turbidity maxima and pollutants can be released back into the water column, causing deterioration of water quality (Liao et al., 2015; Seitzinger et al., 2010; Widerlund and Davison, 2007). A coastal estuary is a distinct ecological system, affected not only by salt and fresh water interaction, periodic exposure and resubmergence, but also by direct discharge of urban sewage and land runoff. As a consequence, the cycling of nutrients and pollutants in estuaries is extremely complex (Bottrell et al., 2009; Burton et al., 2011).

Phosphorus (P) and iron (Fe) are essential nutrients for living organisms (Han et al., 2015). Understanding the dynamic interaction between Fe, P and S is key to predicting their biogeochemical fates and impact on water quality. In estuarine sediments rich in organic matter (OM), oxygen is quickly depleted with microbial aerobic respiration below the sediment-water interface, thereby creating an anoxic

environment. Under these conditions, both microbial iron reduction (Taillefert et al., 2000) and sulfate reduction will occur (Burtonet al., 2011). Iron reduction results in the dissolution of iron oxides to ferrous iron, whereas sulfate reduction is where dissolved sulfate is reduced to H_2S. The Fe^{2+} ion can be quickly and effectively removed from pore waters by the formation of FeS and FeS_2, which also removes the toxic H_2S in the sediment-water system (Amirbahman et al., 2003; Azzoni et al., 2005; Taillefert et al., 2000). The biogeochemical reactions of Fe and S also affect both availability of sedimentary P to aquatic organisms and mobility of P within the sediments (Rozan, 2002). Previous studies have shown that the extent of P release is thought to be controlled either by the redox conditions at the sediment-water interface and/or by the formation of authigenic P minerals in supersaturated pore waters (Abdel-Satar and Sayed, 2010; Ruttenberg and Berner, 1993; Rozan, 2002). It is widely accepted that reductive dissolution of iron oxides is a major mechanism responsible for the release of P (Ruttenberg and Berner, 1993; Rozan, 2002). The reduction of FeOOH in freshwater and marine sediments is predominately responsible for the release of PO_4^{3-} to the pore water and potentially then to the overlying water and the released Fe:P ratio in freshwater sediments is much higher than that in coastal sediments (Gunnars and Blomqvist, 1997). Estuaries are zones with high turbidity so sediment resuspension and flocculation can both reoxidise anoxic bed sediments and provide fresh sorption surfaces for P removal (Seitzinger et al., 2010; Statham, 2012). Therefore, changes in sediment redox conditions and sulfide production have a significant effect on the P cycling in coastal sediments and overlying waters (Bebie et

al., 1998; Rozan, 2002).

Traditional chemical extractions (e.g., sediment core sequential extraction and analysis) are based on an operationally defined response to chemical reagents rather than on a true and *in situ* reflection of the lability of chemical species of interest (Stockdale et al., 2009). In contrast, the diffusive gradients in thin films technique (DGT) is an *in situ*, dynamic method capable of rapid measurements of labile P, Fe, and other analytes at high spatial resolution (Zhang et al., 2001; Ding et al., 2011; Lucas et al., 2015). It usually consists of a binding phase overlain by a well defined diffusion phase. A concentration gradient is rapidly established within the diffusive layer and maintained during the period of the DGT deployment (Zhang et al., 2001; Ding et al., 2012). The flux of an ion through the gel is quantified by Fick's first law of diffusion (Zhang et al., 1995). The DGT technique has become potentially powerful tool for measuring the supply of key ions from the solid phase to the pore water, which can help to undertand reactivity and bioavailability of key elements (Ding et al., 2011, 2012). The flux of solute from pore water to DGT resin can be used to evaluate concentration of labile fractions in pore water or to quantify the sediment-porewater remobilization flux (Wu et al., 2015).

The objectives of this study were to investigate profiles of vertical fluxes of dissolved S^{2-}, Fe^{2+} and dissolved reactive phosphorus (DRP) in intertidal and freshwater sediments from a municipal river estuary heavily polluted by the long term discharge of urban sewage and industrial wastewater (Yantai, China), in order to reveal the potential differences in the interaction and release mechanisms of S, Fe and

89 P in these two types of heavily polluted environment.

90 **2. Materials and methods**

91 **2.1 Study area**

92 The Yuniao River is a sewage-rich river originating from the Muping City urban
93 area (0.4 million population), carrying about 60% of the municipal sewage of the city.
94 The river is located in the northeastern Shandong province in northern China
95 (37°23'35"N,121°33'59"E; Fig. 1). The climate in the study area is cold and dry in
96 spring and winter, and warm and wet in summer and autumn, and is characterized by
97 annual precipitation of ~737 mm and anaverage temperature of 11.6°C. The Yuniao
98 River is a typical seasonal river, with domestic and industrial wastewater discharge
99 accounting for most of the river water during the dry season. The river bed sediment
100 is dominated by clay and silt. Based on the data from local Environmental Protection
101 Bureau, the overlying water and sediments are rich in OM (total organic carbon (TOC)
102 of sediments reached ~10%) because of long term pollution. The annual maximum
103 value of chemical oxygen demand (COD_{Cr}) was ~ 400 mgL^{-1},which, when compared
104 with the lowest Chinese Water Standard level V (40mg L^{-1}) (SEPA, 2002), indicates
105 that the river is seriously polluted.

106

107 **Fig.1.**

108

109 **2.2 Sample collection and analysis**

110 Sample collection was carried out on 20th June, 2015. Water samples were

collected from two sites, one intertidal (INT) site located in the estuary and one freshwater (FW) site further upstream. At both of these sites, the river water was characterized by blackening and sulfurous odor. Water quality parameters were determined by a portable multi-parameter water quality analyzer (YSI Professional Plus). NH_4^+-N, NO_3^--N, PO_4^{3-}-P and total phosphorus (TP) were analyzed by a continuous flow analyzer (AutoAnalyzer III, Seal, Germany). Chemical oxygen demand (COD_{Cr}, acid COD_{Mn} and alkaline COD_{Mn}) were measured with the corresponding method specified in the standard methods by APHA (2005). In brief, this involved the dichromate titration method for COD_{Cr}, acid and alkaline permanganate titration method foracid COD_{Mn} and alkaline COD_{Mn} respectively. The concentrations of SO_4^{2-} and Cl^- in overlying water and pore water were (centrifugated from surface sediments) were analyzed by an ion chromatograph (Dionex ICS3000, DIONEX, USA) on triplicate samples. Dissolved oxygen (DO) and oxidation reduction potential (ORP) in sediment pore water profile were measured *in situ* by micro profilers (Unisense Microsensor, Denmark). The DO microsensor is a miniaturized Clark-type oxygen sensor with a guard cathode and the ORP microelectrode is a miniaturized platinum electrode; both parameters were measured in the superficial 0-5 cm sediment horizon. The FW site was chosen where the water depth is ~0.5 m and was located upstream of a dam, which was built to prevent the flood tide. The INT site was chosen at a shallow beach of Yuniao River estuary. The data of the INT site were collected at low tide when the overlying water was a mix of seawater and freshwater (water depth ~0.3 m). The profiler, mounted on a tripodal

frame, was settled on the river bed by divers with minimum disturbance of the sediment. A minimum time of 30 min was allowed before the measurement program was conducted (Stief et al., 2002).

2.3 Application of the DGT technique

The fluxes of DRP and dissolved sulfide in the sediment profiles were determined *in situ* using an innovative DGT technique (Ding et al., 2011). An improved ZrO-AgI binding gel was used in this DGT technique, which incorporated AgI particles into the zirconium oxide binding gel previously used in the DGT measurement of DRP, achieving simultaneous measurements of DRP and dissolved sulfide (Ding et al., 2012). The fluxes of DRP and sulfide trapped in the binding gel were determined by a conventional slice elution procedure and a computer-imaging densitometry technique, respectively (Di et al., 2012; Ding et al., 2011). The conventional slice extraction procedure involves DGT uptake of P in sediments, 2D slicing of the binding gel on a grid system, elution of P from each gel square with 1M NaOH, and microcolorimetric determination of DRP in each eluted solution using 384-microwell plates (Ding et al., 2012). The fluxes of Fe^{2+} were also determined by Chelex binding gel DGT with a separate probe (Di et al., 2012). DGT probes were deoxygenated with nitrogen for 16 h by placing them in a container filled with deoxygenated 0.03 M $NaNO_3$ before being transported to their sampling sites. A thin layer of white sponge was glued at the back of probes to record the position of the sediment-water interface through staining. The probes were smoothly inserted through the sediment-water interface at the site by hand with disposable gloves (medical

grade). After deployment for 24h, the DGT probes were retrieved by hand with gloves, rinsed thoroughly with deionized water, and then brought to the laboratory for processing (Ding et al., 2012).

In the laboratory the DGT probes were carefully taken apart, marking the location of the sediment-water interface using a ceramic knife; the binding gel was taken out and rinsed thoroughly with deionized water before drying its surface with filter paper (0.1 mm thick-ness, Millipore, Billerica MA). The ZrO-AgI binding gel was then scanned (resolution set 600 dpi, 0.042*0.042mm) and its image converted to grayscale intensity to measure sulfide using a S^{2-} calibration (Ding et al., 2012). Further measurements of DRP were undertaken using procedures developed by Ding et al. (2011, 2012). The ZrO-AgI gels were sliced at 1mm intervals, and each piece eluted with 40μL of 1 mol L^{-1} NaOH. The Chelex binding gel measurements of Fe^{2+} were also sliced at 1mm intervals, and each piece eluted with 40μL of 1 mol L^{-1} HNO_3. The concentrations of the DRP and Fe^{2+} in the elution solutions were determined by micro colorimetric methods using 384-microwell plates.

2.4 Calculations

DGT measures directly the mean flux of labile species to the device during the deployment. This can be interpreted as the mean concentration of labile analyte at the interface between the device surface and the sediment, during the deployment. When supply from sediment particles to solution is rapid, this interfacial concentration is the same as the concentration of labile species in bulk pore-water (Zhang et al., 2001).

The accumulation mass of P (*M*) in the binding gel is calculated according to the

177 equation:

178 $$M = \frac{C_e(V_g+V_e)}{f_e} \quad (1)$$

179 Where C_e is the concentration of P or Fe^{2+} in the known volume of eluting solution
180 (V_e), V_g is the volume of the gel, and f_e is the elution factor of the analytes eluted from
181 the binding gel, typically 0.8. The accumulation mass of sulfide was calculated using
182 the exponential equation established from the calibration procedure (Ding et al., 2011).
183 The exponential equationis as follow:

184 $$y = -166e^{-x/8.73} + 225 \quad (2)$$

185 Where x is the accumulation mass of sulfide per unit area, y is the corresponding
186 gray scale intensity.

187 The fluxes (F) of the DRP, dissolved sulfide and Fe^{2+} measured by the DGT in
188 sediment were calculated using the following equation:

189 $$F = \frac{M}{A_t} \quad (3)$$

190 Where A is the surface area of the diffusive layer in contact with the sediment
191 (A=0.18 cm^2), *t* is the deployment time (s) (Ding et al., 2012; Krom et al., 2002).

192 The concentrations of the DRP, dissolved sulfide and Fe^{2+} measured by the DGT
193 (C_{DGT}) were calculated using the following equation:

194 $$C_{DGT} = \frac{F\Delta g}{D} \quad (4)$$

195 Where Δg is the thickness of the diffusive layer (0.8mm), D is the diffusion
196 coefficient of P ($6.89*10^{-6}cm^{-2}\ s^{-1}$), dissolved sulfide ($7*10^{-6}cm^{-2}\ s^{-1}$) and Fe^{2+}
197 ($6.96*10^{-6}cm^{-2}\ s^{-1}$) in the diffusive layer. All of the data were graphically plotted using
198 the software Origin 8.0.

3. Results and Discussion

3.1 Overlying water quality in study areas

The water quality indicators in the overlying water samples are presented in Table 1. The concentrations of COD_{Cr} and NH_4^+-N were higher than the minimum Chinese water standard level V(COD_{Cr} 40 mg L^{-1}, NH_4^+-N 2mg L^{-1}, SEPA, 2002) and other rivers in this region (Li et al., 2015), reflecting that the Yuniao River is heavily polluted due to a long term discharge of urban sewage and wastewater. The salinity of the INT site was 16 PSU at low tide.

Table 1

Although the measured COD_{Cr} value at the FW site (63mg L^{-1}) was lower than that in the INT site (179 mg L^{-1}), the latter is subject to error due to the high salinity because COD_{Cr} is unreliable above 5 PSU (Li et al., 2015).

3.2 Variations of DO and ORP in pore water

DO variations in pore water in the study areas are shown in Fig.2. In both the INT and FW areas, DO decreased with depth from surface values of 5.6mg L^{-1} and 6.8mg L^{-1} respectively to a penetration depth of approximately 0.3 cm where DO levels were near zero. The result indicates all sediments below 0.3 cm were anoxic (without adequate free oxygen in porewater). The graph shows a small concentration fluctuation at about 1.2cm in the FW site DO profile which may be caused by intersecting a macrofauna burrow (Mortimer et al., 1999).

Figure 2

For the variations of ORP in the pore water, a strong redox boundary was seen in the FW site around 0.5cm (Fig.3), which is consistent with the pore-water DO profile. The oxygen penetration depth is governed by the rate of diffusion of oxygen into the sediment, balanced with consumption by microbial respiration of OM therein. However, in the INT site sediment, the ORP showed a steady decrease in redox with depth without a pronounced redox boundary (Fig.3). This could be attributed to the INT site sediments being subjected to repeated tidal flushing and some sediment remobilization, both of which lead to a degree of oxidation, preventing the formation of a steep redox boundary (Hupfer et al., 2007).

Fig. 3

3.3 Profiles of Fe^{2+} in different sediments

The vertical fluxes of dissolved Fe^{2+} in the INT and the FW sites sediment are shown in Fig.4. At the INT site, the flux of Fe^{2+} varied from 0.49 to 1.65×10^{-6}μmol cm^{-2} s^{-1}, remaining within this narrow range throughout, with a slight peak around 3cm. At the FW site, the pattern of Fe^{2+} flux was similar to the INT site in the top 6 cm of sediment, with a small increase around 3cm. It then showed increased flux values with depth below 6cm, and markedly increased fluxes from 10cm to a

maximum of 22.94×10^{-6}μmol cm^{-2} s^{-1} at 14cm. A significant redox boundary was present around 10cm (Heijs et al., 1999).

Fig. 4

Generally, $Fe^{2+}$is only produced by iron reduction through bacteria(Eq. (5)) or by sulfide reacting with dissolved iron, iron oxides, and potentially other iron minerals (Eqs. (6) and (7)) (Mortimer et al., 2011; Zhu et al., 2015; Heijs et al., 1999).

$$CH_2O + 4FeOOH = FeCO_3 + 3Fe^{2+} + 6OH^- \quad (5)$$

$$S^{2-} + 2Fe(III) = S^0 + 2Fe^{2+} \quad (6)$$

$$2S^{2-} + 2Fe^{2+} = 2FeS \quad (7)$$

Therefore, the low Fe^{2+} fluxes in INT site (Fig. 4) probably indicate where most dissolved iron was fixed by free sulfide due to the formation of FeS (Zhu et al., 2015). However, in the FW site, the flux of Fe^{2+} increases sharply at 10cm, suggesting either a new source of iron supply to the pore water or the cessation of a sink process. Alternatively, the sink process may have become rate limited, allowing the DGT device to outcompete it for Fe. It is also possible that the sediment at this depth contains higher levels of buried iron oxides, which would drive rapid microbial iron reduction (Mortimer et al., 2011). In most sediments, sulfate reduction is the dominant microbial process, the H_2S produced reduces Fe(III) oxides, or reatcs with dissolved Fe^{2+} produced by iron reduction, leading to the formation of FeS. Previous work has

suggested that due to rapid burial conditions in coastal/estuarine sediments, labile iron oxides can become buried before being reduced, providing a pool for enhanced microbial iron reduction at depth (Coleman et al., 1993; Mortimer et al., 2011).

3.4 Fluxes of dissolved sulfide in different sediments

The dissolved sulfide profiles of the sediments in the INT and FW sites are shown in Fig.5. There was a significant difference in the flux of dissolved sulfide between the sites. In the FW site, the sulfide flux increased with depth to around 0.5 - 2cm, where it reached a maximum value (4.05×10^{-6}μmol cm^{-2} s^{-1}); below that fluxes remained consistent, varying between 2.60 and 3.28×10^{-6}μmol cm^{-2} s^{-1}) down to 10cm. Below 10cm there was a minimum (2.27×10^{-6}μmol cm^{-2} s^{-1}) but below that fluxes increased. In comparison, the flux of dissolved sulfide in INT site decreased rather steadily until a depth of around 5cm, where it reached a minimum value (0.89×10^{-6}μmol cm^{-2} s^{-1}); fluxes then increased sharply to 3.44×10^{-6}μmol cm^{-2} s^{-1} at the depth of 7cm, and then remained at ~ 3.0×10^{-6}μmol cm^{-2} s^{-1} between 7cm and 12cm, and eventually increased with depth below 12cm.

Fig. 5

It is widely accepted that sulfide in pore water is mainly produced from sulfate reduction under anoxic conditions. However, in this work, although there was much higher sulfate concentrations in the INT site, sulfide fluxes were similar to those in the FW site (~3.1×10^{-6}μmol $cm^{-2}s^{-1}$). The sulfide flux in the INT site decreased with depth

to 5cm and then increased and remained high. The high sulfide flux in the upper few centimeters suggests that it was in excess and any removal processes did not take out a significant fraction. The decrease with depth suggests that there was a sink process that removes sulfide, or there was less sulfate reduction. It is possible that this was a zone of active iron reduction where any reduced iron removed some of the sulfide. Iron fluxes remained low throughout because there was excess sulfide. Below 6cm there was most likely less available iron, hence sulfide became more readily available throughout the rest of the profile. In comparison, the FW site profile showed a peak in sulfide flux just below the depth of oxygen penetration. This was likely to be the zone of maximum rates of sulfate reduction (Bottrell et al., 2009). Throughout the rest of the profile, the sulfide flux remained relatively stable, probably as a result of the source and sink processes remaining balanced. At 10cm depth, the sulfide flux displayed a narrowly defined decrease concident with the increase in iron flux, suggesting that there was sufficient iron present to react with much of the sulfide, even if over a limited depth.

Sets of Fe and sulfide flux profiles were the net result of both production processes (microbial iron reduction and microbial sulfate reduction), removal processes (reaction of dissolved iron and sulfide to form FeS), processes that combine both (reaction of sulfide with iron minerals that removes sulfide and produces iron), and sampling artefacts (DGT competes for removal of iron and sulfide with natural processes).

3.5 DRP in pore water in different areas

As shown in Fig.6, there was a significant difference of DRP fluxes to the sediment pore water for the two sites. The flux of DRP ranged from 9.14 to 19.32×10^{-6}μmol cm^{-2} s^{-1}, and from 2.07 to 16.93×10^{-6}μmol cm^{-2} s^{-1} at the FW and the INT sites respectively. In the INT site, DRP fluxes decreased from the sediment-water interface to ~1cm, reaching a minimum value of 2.07×10^{-6}μmol $cm^{-2}s^{-1}$, then increased from 1 to 6cm to a high value of 16.49×10^{-6}μmol cm^{-2} s^{-1} at ~6cm, then decreased to 9cm, before increasing again below that. DRP availability was low just below the sediment-water interface, which was probably due to sorption of phosphate onto the near surface layer of iron oxides. With increasing depth, conditions became anoxic and more P was produced from OM degradation and/or release of phosphate during reductive dissolution of iron oxides. Interestingly, compared to the variation of sulfide profiles, DRP increase was consistent with sulfide decrease (Fig.4, 0-6cm). This was probably due to this top 6cm being the zone of highest rates of OM degradation by microbial iron reduction, resulting in the production of DRP from both the OM itself and the reductive dissolution of iron oxides (Ruttenberg and Berner, 1993; Rozan, 2002). The iron produced reacts with available sulfide and hence removes it concomitantly with this release of DRP (Hupfer et al., 2007; Kostka and Luther, 1994; Rozan, 2002).

Fig. 6

In the FW site, the DRP flux showed constant values or a slight increase from

sediment-water interface down to 4cm, then a steady decrease until a depth of 10cm, below which values remained relatively steady at ~11.10×10^{-6}μmol cm^{-2} s^{-1}. Generally, P occurrence in pore water is linked to Fe in sediments. However, in the FW site, the iron profile suggested that below 10cm (Fig. 5), there was more Fe^{2+} produced by microbial iron reduction, which should release more P from ferric iron-bound P, yet the DRP flux was rather steady. This result probably indicates that PO_4^{3-} in pore water in such a layer is not from the solid-phase P of ferric iron-bound P (Fe-P) in sediments but instead is from other sources such as P from microbial degradation of OM. In the upper few centimeter of the sediments, degradation of fresh OM has been shown to enhance PO_4^{3-} efflux (Rao et al., 2015; Kraal et al., 2015). However, with increasing depth, little labile OM remains, hence DRP fluxes decrease with depth.

Whilst it is somewhat difficult to interpret the biogeochemistry of these two sites without pore-water concentration data to go with the DGT flux data (e.g. without diffusive equilibrium in thin films (DET) probe conducted synchronously), it seems likely that there is active iron and sulfate reduction throughout both sites. In the INT site system, iron reduction predominates over sulfate reduction over the upper 6cm, and below that the reverse is true. This is because the site is regularly inundated with seawater or brackish water and hence excess sulfate is flushed through the system. However, the fresh/reactive iron oxides are only present near the surface. Phosphate fluxes largely follow the reductive dissolution of iron oxides. In contrast, in the FW site system, sulfate reduction dominates over iron reduction throughout the top 10cm but with especially high rates of sulfate reduction in the top 2cm. Below 10cm, iron

reduction predominates. This system is not inundated with seawater and consequently has a less available sulfate, however, this lack of sulfate means that less sulfide is produced and hence reactive iron can be preserved and buried at depth, supporting later iron reduction. It may also be that the FW sites ystem has experienced a period of rapid iron burial in the past. Phosphate doesn't change much in this system since there is iron reduction (releasing phosphate) throughout the profile.

4. Conclusions

This study investigated vertical fluxes and interaction of S, Fe and P in the INT site and the FW site sediments in a heavily polluted coastal river. The relative rates of microbial iron and sulfate reduction controlled the flux of Fe^{2+}, sulfide and phosphate to the pore waters. At the INT site, iron reduction was the dominant process in the upper part of the sediment and sulfate reduction dominant with depth. In contrast, sulfate reduction was most important in the upper sediment of the FW site, with iron reduction dominant below. Phosphate was released during reductive dissolution of iron oxides. Phosphate release was largely controlled by iron reduction.

Acknowledgments

This study was supported by the National Natural Science Foundation of China (GrantNo.: 41373100). Additional support was provided by Science and Technology Program for Public Wellbeing of Shandong Province (Grant No.:2013kjhm060308) and CAS Key Technology Talent Program. We thank Muping Environmental Protection Bureau for their help with historical data providing of Yuniao River.

373

374 **References:**

375 Abdel-Satar, A.M., Sayed, M.F., 2010. Sequential fractionation of phosphorus in
376 sediments of El-Fayum lakes--Egypt. Environ. Monit. Assess. 169, 169-178.

377 Amirbahman, A., Pearce, A.R., Bouchard, R.j., Norton, S.A., kahl, J.S., 2003.
378 Relationship between hypolimnetic phosphorus and iron release from eleven lakes
379 in maine, usa. Bio.Chem. 65, 369-386.

380 APHA. Standard Methods for the Examination of Water and Wastewater. American
381 Public Health Association-American Water Works Association–Water Environment
382 Federation, 2005.

383 Azzoni, R., Giordani, G., Viaroli, P., 2005. Iron–sulphur–phosphorus Interactions:
384 Implications for Sediment Buffering Capacity in a Mediterranean Eutrophic
385 Lagoon (Sacca di Goro, Italy). Hydrobiol. 550, 131-148.

386 Bebie, J., Schoonen, M.A.A., Fuhrmann, M., Strongin, D.R., 1998. Surface charge
387 development on transition metal sulfides: an electrokinetic study. Geochim.
388 Cosmochim. Acta 62, 633-642.

389 Bottrell, S.H., Mortimer, R.J.G., Davies, I.M., Harvey, S.M., Krom, M.D., 2009.
390 Sulphur cycling in organic-rich marine sediments from a Scottish fjord.
391 Sedimentology 56, 1159-1173.

392 Burton E.D., Bush R.T., Johnston S.G., Sullivan L.A., Keene A.F., 2011. Sulfur
393 biogeochemical cycling and novel Fe-S mineralization pathways in a tidally
394 re-flooded wetland. Geochim. Cosmochim. Acta 75, 3434-3451.

Coleman, M.L., Hedrick, D.B., Lovley, D.R., White, D.C. and Pye, K., 1993. Reduction of Fe(III) in sediments by sulphate-reducing bacteria. Nature, 361, 436-438.

Di, X., Wei, W., Shiming, D., Qin, S., Chaosheng, Z., 2012. A high-resolution dialysis technique for rapid determination of dissolved reactive phosphate and ferrous iron in pore water of sediments. Sci. Total Environ.421, 245–252.

Ding, S., Jia, F., Xu, D., Sun, Q., Zhang, L., Fan, C., Zhang, C., 2011. High-resolution, two-dimensional measurement of dissolved reactive phosphorus in sediments using the diffusive gradients in thin films technique in combination with a routine procedure. Environ. Sci. Technol. 45, 9680-9686.

Ding, S., Sun, Q., Xu, D., Jia, F., He, X., Zhang, C., 2012. High-resolution simultaneous measurements of dissolved reactive phosphorus and dissolved sulfide: the first observation of their simultaneous release in sediments. Environ. Sci. Technol. 46, 8297-8304.

Dittrich, M., Chesnyuk, A., Gudimov, A., McCulloch, J., Quazi, S., Young, J., Winter, J., Stainsby, E., Arhonditsis, G., 2013. Phosphorus retention in a mesotrophic lake under transient loading conditions: Insights from a sediment phosphorus binding form study. Water Res. 47, 1433-1447.

Gunnars, A., Blomqvist, S., 1997. Phosphate exchange across the sediment-water interface when shifting from anoxic to oxic conditions an experimental comparison of freshwater and brackish-marine systems. Bio.Chem. 37, 203-226.

Han, C., Ding, S., Yao, L., Shen, Q., Zhu, C., Wang, Y., Xu, D., 2015. Dynamics of

417 phosphorus–iron–sulfur at the sediment–water interface influenced by algae blooms
418 decomposition. J. Hazard. Mater. 300, 329-337.
419 Heijs, S.K., Jonkers, H.M., van Gemerden, H., Schaub, B.E.M., Stal, L.J., 1999. The
420 buffering capacity towards free sulfide in sediments of a coastal lagoon (Bassin d′
421 Arcachon France)-the relative importance of chemical and biological processes.
422 Estuar. Coast. Shelf Sci. 49, 21-35.
423 Hupfer, M., Gloess, S., Grossart, H., 2007. Polyphosphate-accumulating
424 microorganisms in aquatic sediments. Microbial Ecol. 47, 299-311.
425 Kostka, J.E., Luther Iii, G.W., 1994. Partitioning and speciation of solid phase iron in
426 saltmarsh sediments. Geochim. Cosmochim. Acta 58, 1701-1710.
427 Kraal, P., Burton, E.D., Rose, A.L., Kocar, B.D., Lockhart, R.S., Grice, K., Bush, R.T.,
428 Tan, E., Webb, S.M., 2015. Sedimentary iron-phosphorus cycling under contrasting
429 redox conditions in a eutrophic estuary.Chem. Geol. 392, 19-31.
430 Krom, M.D., Mortimer, R.J.G., Poulton, S.W., Hayes, P., Davies, I.M., Davison, W.,
431 Zhang, H., 2002. In-situ determination of dissolved iron production in recent
432 marine sediments. Aquat. Sci. 64, 282-291.
433 Liao, Q., Wang, B., Wang, P.-F., 2015. In situ measurement of sediment resuspension
434 caused by propeller wash with an underwater particle image velocimetry and an
435 acoustic doppler velocimeter. Flow Meas. Instrum. 41, 1-9.
436 Lucas, A.R., Ursula Salmon, S., Rate, A.W., Larsen, S., Kilminster, K., 2015. Spatial
437 and temporaldistribution of Au and other trace elements in an estuary usingthe
438 diffusive gradients in thin films technique andgrab sampling, Geochim. Cosmochim.

439 Acta 171, 156-173.
440 Mortimer, R.J.G., Davey, J.T., Krom, M.D., Watson, P.G., Frickers, P.E., Clifton, R.J.,
441 1999. The Effect of Macrofauna on Porewater Profiles and Nutrient Fluxes in the
442 Intertidal Zone of the Humber Estuary. Estuar. Coast. Shelf S. 48, 683-699.
443 Mortimer, R.J.G., Galsworthy, A.M.J., Bottrell, S.H., et al., 2011. Experimental
444 evidence for rapid biotic and abiotic reduction of Fe (III) at low temperatures in salt
445 marsh sediments: a possible mechanism for formation of modern sedimentary
446 siderite concretions. Sedimentology 58, 1514-1529.
447 Rao, A.M.F., Malkin, S.Y.,Hidalgo-Martinez, S., Meysman, F.J.R.,2016.The impact of
448 electrogenic sulfide oxidation on elemental cycling and solute fluxes in coastal
449 sediment. Geochim. Cosmochim. Acta 172, 265-286.
450 Rozan, T.F., Taillefert, M., Trouwborst, R.E., Glazer, B.T., Ma, S.F., Herszage, J.,
451 Valdes, L.M., Price, K.S., Luther, G.W., 2002. Iron-sulfur-phosphorus cycling in
452 the sediments of a shallow coastal bay: Implications for sediment nutrient release
453 and benthic macroalgal blooms. Limno. oceanogr. 47, 1346-1354.
454 Ruttenberg, K.C., Berner, R.A., 1993. Authigenic apatite formation and burial in
455 sediments from non-upwelling, continental margin environments. Geochim.
456 Cosmochim. Acta 57, 991-1007.
457 Seitzinger, S.P., Mayorga, E., Bouwman, A.F., Beusen, A.H.W., Kroeze, C., Vancht,
458 G., Dumont, E., Fekete, B.M., Garnier, J., Harrison, J.A., 2010. Global river
459 nutrient export: scenario analysis of past and future trends (Invited). American
460 Geophysical Union 24, 2621-2628.

461 SEPA, 2002. Environmental quality standards for surface water (GB 3838-2002).
462 China Environmental Sciences Press, Beijing, China.
463 Sheng, Y., Sun, Q., Bottrell, S.H., Mortimer, R.J.G., Shi, W., 2013. Anthropogenic
464 impacts on reduced inorganic sulfur and heavy metals in coastal surface sediments,
465 north Yellow Sea. Environ. Earth Sci. 68, 1367-1374.
466 Statham, P.J., 2012. Nutrients in estuaries - An overview and the potential impacts of
467 climate change. Sci. Total Environ. 434, 213-227.
468 Stief, P., Beer, D., Neumann, D., 2002. Small-Scale Distribution of Interstitial Nitrite
469 in Freshwater Sediment Microcosms: The Role of Nitrate and Oxygen Availability,
470 and Sediment Permeability. Microb. Ecol. 43, 367-377.
471 Stockdale, A., Davison,W. and Zhang, H., 2009. Micro-scale biogeochemical
472 heterogeneity in sediments: A review of available technology and observed
473 evidence. Earth Sci. Rev. 92, 81-97.
474 Taillefert, M., Bono, A.B., Luther, G.W., 2000b. Reactivity of freshly formed Fe(III)
475 in synthetic solutions and (pore) waters: voltammetric evidence of an aging process.
476 Environ. Sci. Technol. 34, 2169-2177.
477 Widerlund, A., Davison, W., 2007. Size and density distribution of sulfide-producing
478 microniches in lake sediments. Environ. Sci. Technol. 41, 8044-8049.
479 Wu, Z., Wang, S., Jiao, L., 2015. Geochemical behavior of metals- sulfide-phosphorus
480 at SWI (sediment/water interface) assessed by DGT (Diffusive gradients in thin
481 films) probes. J. Geochem. Explor. 156, 145-152.
482 Zhang, H., Davison, W., Miller, S.and Tych, W., 1995. *In situ* high

resolutionmeasurements of fluxes of Ni, Cu, Fe and Mn and concentrations of Zn and Cd inporewaters by DGT. Geochim. Cosmochim. Acta 59, 4181-4192.

Zhang, H., Zhao, F.J., Sun, B., Davison, W., Mcgrath, S.P., 2001. A new method to measure effective soil solution concentration predicts copper availability to plants. Environ. Sci. Technol. 35, 2602-2607.

Zhu, M.-X., Huang, X.-L., Yang, G.-P., Chen, L.-J., 2015. Iron geochemistry in surface sediments of a temperate semi-enclosed bay, North China. Estuar. Coast.Shelf S. 165, 25-35.

493 Table1.Water quality indicators in the INT site and the FW site

Item	Unit	FW site	INT site
Temp	°C	31.8	29.9
COD_{Cr}	mg L^{-1}	63.2	179.2
COD_{Mn}	mg L^{-1}	25	6
NH_4^+-N	mg L^{-1}	6.82	2.71
NO_3^--N	mg L^{-1}	0.13	0.11
PO_4^{3-}-P	mg L^{-1}	0.01	0.03
TP	mg L^{-1}	0.28	0.29
DO	mg L^{-1}	5.76	5.43
Cond.	mScm^{-1}	2.45	29.75
Salinity	PSU	1.09	16.26
pH	/	8.15	7.87
ORP	mv	170	164
SO_4^{2-}	mg L^{-1}	50.07	1965.53
Cl^-	mg L^{-1}	272.94	16311.43
Porewater SO_4^{2-}	mg L^{-1}	379.88	1243.52
Porewater Cl^-	mg L^{-1}	58.64	16354.93

494

495

496

Figure captions:

Fig.2. Detailed locations of sampling sites

Fig.3. *In situ* pore water DO profiles in the INT site (A) and the FW site (B) pore water

Fig.3. Vertical variations of ORP in the INT site (A) and the FW site (B) sediments

Fig.4. The vertical DGT fluxes (F_{DGT}) of Fe^{2+} in the INT site (A) and the FW site (B) sediment profiles

Fig.5. The vertical DGT fluxes (F_{DGT}) of sulfide in the INT site (A) and the FW site (B) sediment profiles

Fig.6. The vertical DGT fluxes (F_{DGT}) of DRP in the INT site (A) and the FW site (B) sediment profiles

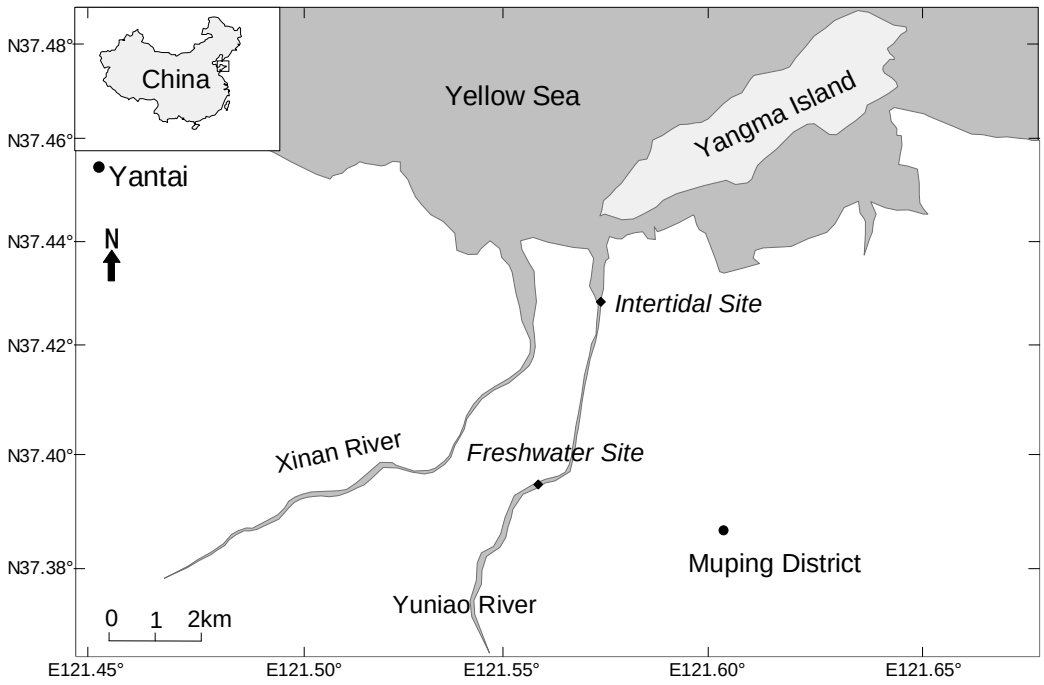
China
Yellow Sea
Yangma Island
Yantai
N
Intertidal Site
Xinan River
Freshwater Site
Muping District
Yuniao River
0 1 2km
N37.48°
N37.46°
N37.44°
N37.42°
N37.40°
N37.38°
E121.45°
E121.50°
E121.55°
E121.60°
E121.65°

Fig.4.

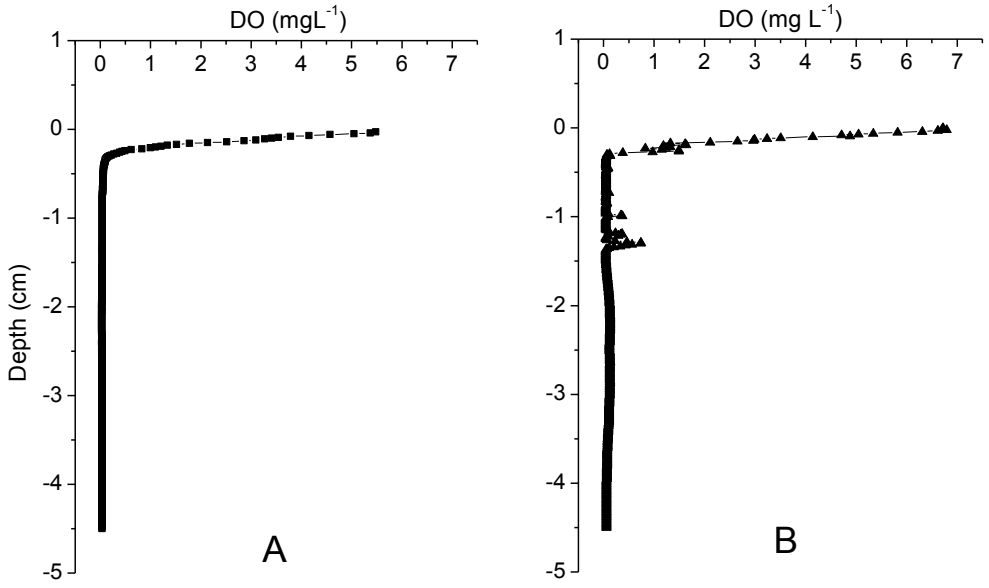

Fig.5.

520

521

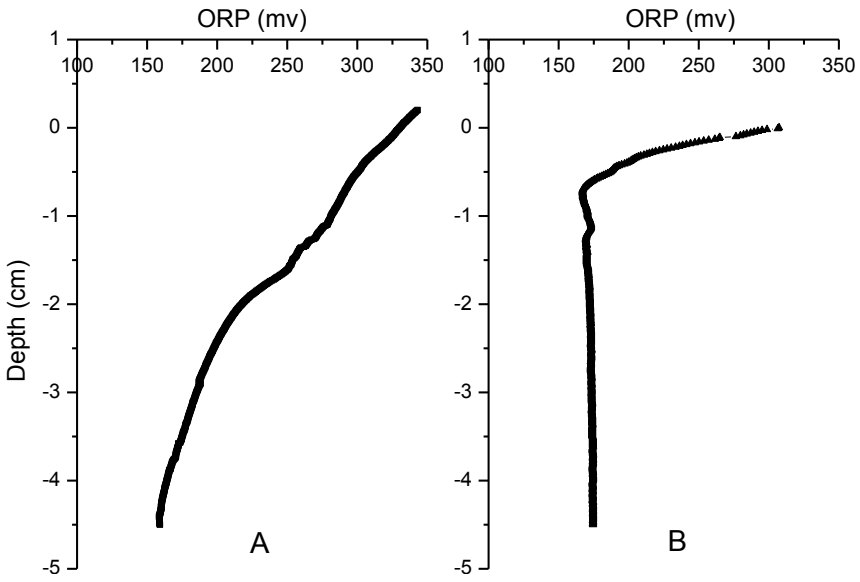

522

523

524 **Fig.3.**

525

526

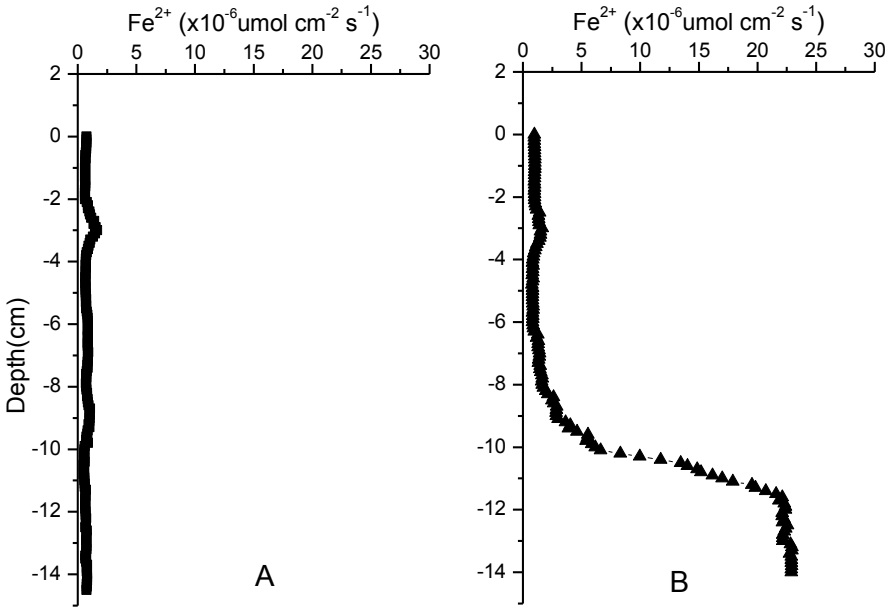

527

528

529 **Fig.4.**

530

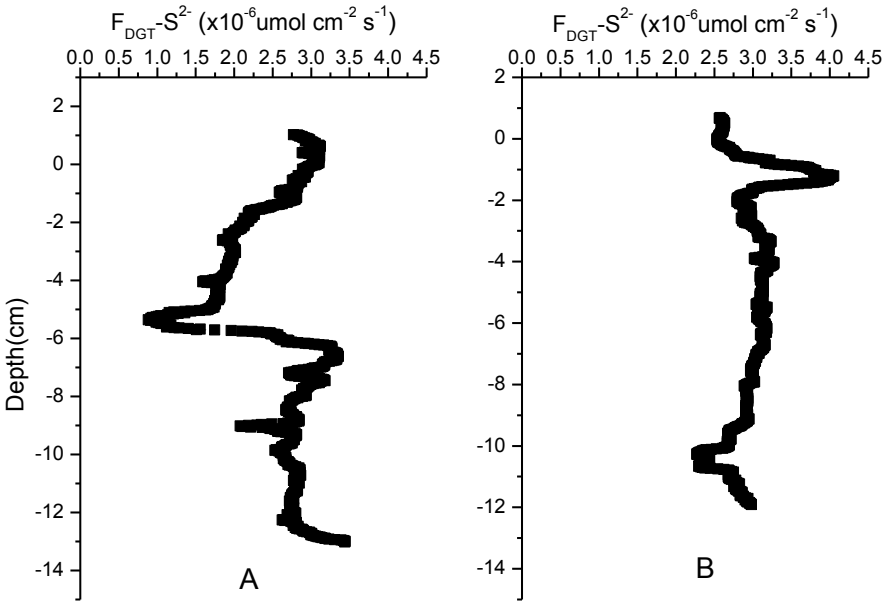
F_DGT-S2- (x10-6umol cm-2 s-1)
0.0 0.5 1.0 1.5 2.0 2.5 3.0 3.5 4.0 4.5
2
0
-2
-4
-6
-8
-10
-12
-14
Depth(cm)
A
F_DGT-S2- (x10-6umol cm-2 s-1)
0.0 0.5 1.0 1.5 2.0 2.5 3.0 3.5 4.0 4.5
2
0
-2
-4
-6
-8
-10
-12
-14
B

Fig.5.

536

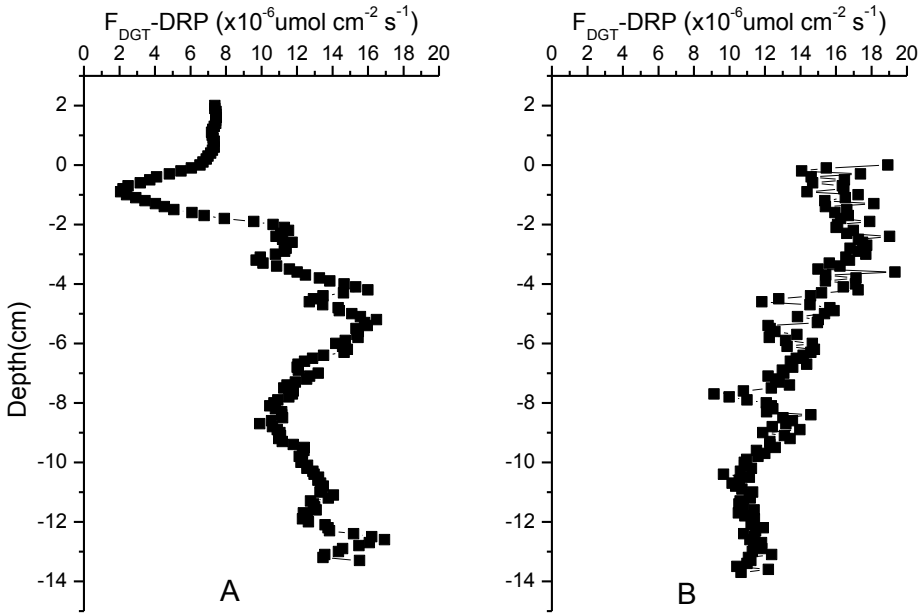

537

538

539 **Fig.6.**

540